Oceanic distribution of inorganic germanium relative to silicon: Germanium discrimination by diatoms

Jill Sutton,[1] Michael J. Ellwood,[1] William A. Maher,[2] and Peter L. Croot[3]

Received 5 October 2009; revised 20 January 2010; accepted 4 February 2010; published 26 June 2010.

[1] Seventeen inorganic germanium and silicon concentration profiles collected from the Atlantic, southwest Pacific, and Southern oceans are presented. A plot of germanium concentration versus silicon concentration produced a near-linear line with a slope of 0.760×10^{-6} (±0.004) and an intercept of 1.27 (±0.24) pmol L^{-1} ($r^2 = 0.993$, $p < 0.001$). When the germanium-to-silicon ratios (Ge/Si) were plotted versus depth and/or silicon concentrations, higher values are observed in surface waters (low in silicon) and decreased with depth (high in silicon). Germanium-to-silicon ratios in diatoms ($0.608–1.03 \times 10^{-6}$) and coupled seawater samples ($0.471–7.46 \times 10^{-6}$) collected from the Southern Ocean are also presented and show clear evidence for Ge/Si fractionation between the water and opal phases. Using a 10 box model (based on PANDORA), Ge/Si fractionation was modeled using three assumptions: (1) no fractionation, (2) fractionation using a constant distribution coefficient (K_D) between the water and solid phase, and (3) fractionation simulated using Michaelis-Menten uptake kinetics for germanium and silicon via the silicon uptake system. Model runs indicated that only Ge/Si fractionation based on differences in the Michaelis-Menten uptake kinetics for germanium and silicon can adequately describe the data. The model output using this fractionation process produced a near linear line with a slope of 0.76×10^{-6} and an intercept of 0.92 (±0.28) pmol L^{-1}, thus reflecting the oceanic data set. This result indicates that Ge/Si fractionation in the global ocean occurs as a result of subtle differences in the uptake of germanium and silicon via diatoms in surface waters.

Citation: Sutton, J., M. J. Ellwood, W. A. Maher, and P. L. Croot (2010), Oceanic distribution of inorganic germanium relative to silicon: Germanium discrimination by diatoms, *Global Biogeochem. Cycles*, *24*, GB2017, doi:10.1029/2009GB003689.

1. Introduction

[2] The cycling of inorganic germanium (hereafter referred to as germanium) in the ocean closely resembles that of silicon [*Froelich and Andreae*, 1981; *Ellwood and Maher*, 2003]. Profiles of dissolved germanium concentration versus depth are almost identical to that of silicon, and when the two are plotted against each other a near linear relationship ($r^2 = 0.99$, $p < 0.001$) is obtained [*Ellwood and Maher*, 2003; *Froelich and Andreae*, 1981; *Froelich et al.*, 1989; *McManus et al.* 2003; *Santosa et al.*, 1997]. Although germanium mimics silicon in the ocean, differences in geochemical behavior occur. For example, in rivers the germanium-to-silicon ratios (Ge/Si) range between 0.1 and 1.2×10^{-6} [*Filippelli et al.*, 2000; *Froelich et al.*, 1992; *Mortlock and Froelich*, 1987], whereas hydrothermal sources have a range of $8–14 \times 10^{-6}$ [*Mortlock et al.*, 1993].

[3] In addition to its inorganic cycle, germanium is also known to be present in seawater as monomethylgermanium (MMGe) and dimethylgermanium (DMGe) [*Ellwood and Maher*, 2003; *Jin et al.*, 1991; *Lewis et al.*, 1985]. Both MMGe and DMGe are nonreactive, which results in both compounds having conservative concentration profiles versus depth. MMGe and DMGe concentration profiles range between 300 and 350 pmol L^{-1} and 90–120 pmol L^{-1}, respectively [*Ellwood and Maher*, 2003; *Lewis et al.*, 1989, 1986, 1985]. Although MMGe and DMGe concentrations are considerably higher than that of inorganic germanium in surface waters, they do not appear to be produced or degrade on a timescale that is likely to influence the inorganic germanium cycle. Essentially, they are biologically and chemically inert under normal oceanic conditions [*Lewis et al.*, 1989, 1988].

[4] Siliceous organisms, such as diatoms, can be measured for Ge/Si $\times 10^{-6}$ giving insight into processes related to oceanic circulation of nutrients and potentially the historical distribution of silicon [*Froelich et al.*, 1989; *King et al.*, 2000; *Froelich et al.*, 1992; *Mortlock and Froelich*, 1987; *Hammond et al.*, 2000]. Several studies have shown that

[1] Research School of Earth Sciences, Australian National University, Canberra, ACT, Australia.
[2] Ecochemistry Laboratory, Applied Science and Institute for Applied Ecology, University of Canberra, Canberra, ACT, Australia.
[3] FB2: Marine Biogeochemistry, IFM-GEOMAR, Leibniz-Institut für Meereswissenschaften, Kiel, Germany.

0886-6236/10/2009GB003689

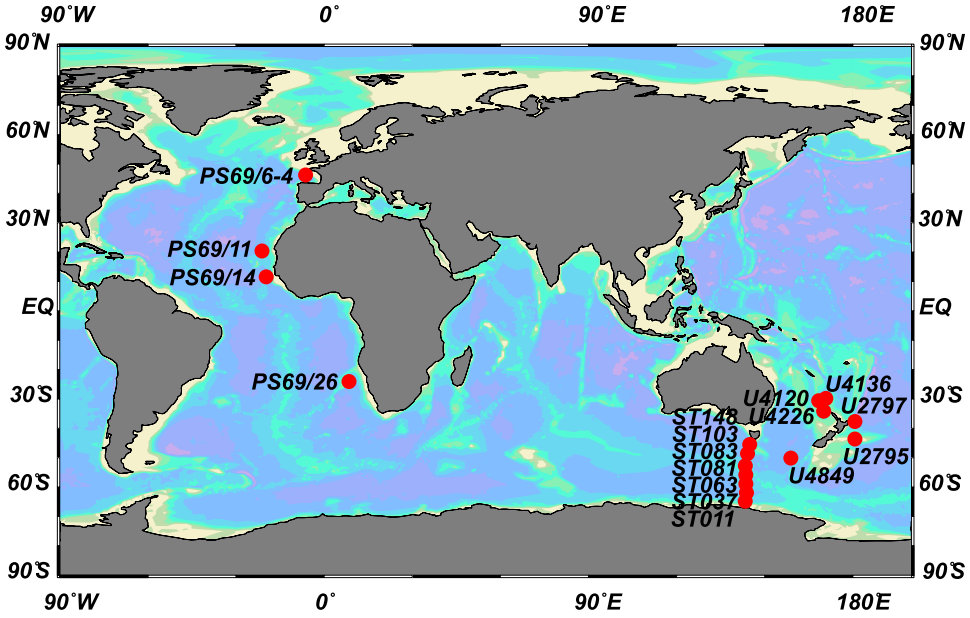

Figure 1. Map showing the location of sampling stations (circles) in this study.

small diatoms (10–40 μm) isolated from Holocene sediments appear to accurately reflect their surrounding seawater Ge/Si [*Froelich et al.*, 1989; *Shemesh et al.*, 1988, 1989]. Accordingly, the Ge/Si record for the Southern Ocean was reconstructed for ~450,000 years showing distinct differences between the interglacial ($0.70–0.78 \times 10^{-6}$) and glacial periods ($0.45–0.60 \times 10^{-6}$) [*Bareille et al.*, 1998; *Mortlock et al.*, 1991]. The decline in the Ge/Si during glacial periods has been explained as either an increase in silicon or decrease in germanium input to the ocean and has been rationalized by the potential for changes in weathering [*Froelich et al.*, 1992; *Kurtz et al.*, 2002]. However, it is difficult to predict changes in these elemental inputs simply by investigating the Ge/Si since neither of the historic oceanic inventories can be constrained. Recent investigations have also challenged that the interglacial-glacial Ge/Si fluctuations may simply represent changes in the amount of germanium lost from the ocean via the nonopaline sink [*Hammond et al.*, 2004, 2000; *King et al.*, 2000; *McManus et al.*, 2003]. Further, it has been suggested that diatoms do discriminate against germanium during uptake [*Murnane and Stallard*, 1988; *Froelich et al.*, 1989, *Azam et al.*, 1973; *Azam and Volcani*, 1974]; especially notable in the frustules of larger diatoms (>40 μm) [*Shemesh et al.*, 1989] and when silicon concentrations of seawater are low [*Ellwood and Maher*, 2003]. This discrimination against germanium would cause a fractionation between the Ge/Si of seawater and diatoms.

[5] *Ellwood and Maher* [2003] observed that inorganic silicon relative to germanium was depleted in surface waters and implied that germanium uptake and/or sequestration is discriminated by phytoplankton, namely diatoms. However, previous work on the uptake of germanium and silicon in diatoms has yielded mixed conclusions on germanium discrimination. For example, *Froelich et al.* [1992] found that germanium discrimination does not occur when diatoms are grown in a medium high in silicon concentration (100 μM). Alternatively, *Shemesh et al.* [1989] found that large diatoms (>38 μm) tend to have lower Ge/Si than small diatoms, and *Mehard et al.* [1974] found that Ge/Si fractionation occurs at the organelle level.

[6] The current study examined inorganic germanium and silicon concentration profiles collected worldwide and Ge/Si $\times 10^{-6}$ data from diatoms collected in the Southern Ocean. The Southern Ocean was chosen as the field site for the collection of coupled diatom and seawater data as it is a "natural" laboratory for oceanic silicon research with concentration gradients stratified by latitude (higher concentrations at higher latitudes). A 10 box model (based on PANDORA [*Broecker and Peng*, 1987]) run as an open system is used to model Ge/Si fractionation. Three types of fractionation were considered including (1) no fractionation, (2) Rayleigh distillation with a constant distribution coefficient (K_D), and (3) Michaelis-Menten process with a variable K_D.

2. Methods

2.1. Seawater and Diatom Sample Collection

[7] Seawater samples were collected using Niskin bottles attached to a standard rosette conductivity-temperature-depth (CTD) unit from 17 locations in the Atlantic Ocean, South Pacific Ocean and the Southern Ocean (Figure 1 and Table 1). After collection, samples were filtered through polycarbonate 0.45 μm filters (Millipore) and stored in acid-cleaned, low-density polyethylene bottles.

[8] Diatom samples were collected by filtering 100 L of seawater through 11, 40 and 63 μm polycarbonate filters (Millipore). The phytoplankton were washed from the polycarbonate filters using deionized water and placed into 50 mL polypropylene vials along with 5 mL of 10% hydrogen peroxide to remove any organic material. These

Table 1. Location of Sampling Stations for Depth Profiles[a]

Globe	Station	Latitude	Longitude
ANT	ST011	65.8S	139.7E
ANT	ST037	62.4S	139.8E
ANT	ST063	58.3S	139.9E
ANT	ST081	55.5S	140.7E
ANT	ST083	54.5S	141.3E
ANT	ST103	52.1S	142.7E
ANT	ST148	46.2S	145.5E
SP	SA U2795	46.63S	178.51E
SP	ST U2797	40.99S	178.47E
SP	U4226	36.57S	170.69E
SP	U4136	28.72S	171.12E
SP	U4120	30.04S	168.74E
SP	U4849	52.07S	154.42E
AT	PS69/6–4	45.75N	4.52W
AT	PS69/11	22.50N	20.50W
AT	PS69/14	10.62N	20.13W
AT	PS69/26	25.00N	8.28W

[a]Global locations (Globe) are described to distinguish Antarctic (ANT), South Pacific (SP) and Atlantic (AT) oceans.

samples were then rinsed with deionized water, digested in 10 mL hydrochloric acid and hydrogen peroxide (1 mol L^{-1}/ 10%) and then rinsed again with deionized water and let to dry overnight at 40°C. Samples were inspected microscopically prior to dissolution to ensure that the majority (>95%) of material was diatomaceous and to ensure that there was no clay contamination. The 11–40 μm size fraction was then prepared and measured for both silicon and germanium content.

2.2. Silicon Determination

[9] The concentration of silicon in seawater and diatom samples was determined colorimetrically [*Koroleff*, 1976] using matrix-matched standards to correct for matrix effects. Reproducibility for diatom samples dissolved in NaOH (see section 2.4) was ±2.5% (n = 10) at a concentration of 1000 μmol L^{-1} and was ±1% (n = 10) for seawater samples at a concentration of 20 μmol L^{-1}. The absolute blank for determination of silicon in NaOH digest was <10 μmol L^{-1} and <0.25 μmol L^{-1} for seawater.

2.3. Germanium in Seawater

[10] Germanium concentrations were determined by isotope dilution using an automated hydride generation system attached to an inductively coupled mass spectrometer (ICP-MS, Elan-6000, Perkin Elmer, Australia) following the method outlined by *Ellwood and Maher* [2002]. Briefly, 40 ± 0.001 g of seawater was spiked with enriched ^{70}Ge with a target ^{70}Ge/^{74}Ge of 4. Hydrochloric acid (0.09 mol L^{-1}, SigmaAldrich) and oxalic acid (0.01%, Fluka) were added to the spiked sample.

[11] Reproducibility for seawater samples was ±3.5% (n = 10) at a germanium concentration of 150 pmol L^{-1}. The absolute germanium blank associated with the determination of germanium was 0.6 ± 0.1 pmol L^{-1} (S.E.) for seawater (n = 10).

2.4. Germanium in Diatoms

[12] Germanium concentrations were determined by isotope dilution using an automated hydride generation system attached to an inductively coupled mass spectrometer (ICP-MS, Elan-6000, Perkin Elmer, Australia) following the method outlined by *Ellwood and Maher* [2002]. Approximately 10–20 mg of diatom material were dissolved by adding 40 ± 0.001 g of 2 mol L^{-1} sodium hydroxide (Aristar, BDH) prespiked with enriched ^{70}Ge (Chemgas, France) with a target ^{70}Ge/^{74}Ge of 4. Samples were heated at 80°C for 72 h, and cooled. This solution was buffered with hydrochloric acid (2.16 mol L^{-1}, SigmaAldrich) and oxalic acid (0.25%, Fluka) at least 12 h prior to analysis. The samples ^{70}Ge/^{74}Ge varied between 2.5 and 8, with the majority of samples having a ^{70}Ge/^{74}Ge of our target, around 4.

[13] Reproducibility of Ge for diatomaceous earth (consistency standard) samples was ±3% (with the blank representing <1% of the total Ge signal) and 15 ± 1.0 pmol L^{-1} (S.E.) for diatoms (n = 10).

2.5. Ten Box Model (PANDORA)

[14] To model silicon and germanium cycling in the ocean we set up a 10 box model with specific architectural components (box size, water exchange between boxes, and residence time of silicon in the surface ocean) based on the PANDORA model of *Broecker and Peng* [1987] (Figure 2). The inputs and outputs for silicon and germanium in to and out of the model are as follows: the flux of silicon entering the ocean was set to 7.1 × 10^{12} moles yr^{-1} and was composed of four sources: riverine (5.6 × 10^{12} moles yr^{-1}), hydrothermal (0.55 × 10^{12} moles yr^{-1}), submarine weathering (0.4 × 10^{12} moles yr^{-1}) and eolian (0.5 × 10^{12} moles yr^{-1}) [*DeMaster*, 2002; *Hammond et al.*, 2004; *King et al.*, 2000; *Treguer et al.*, 1995]. The model was then initiated and the remineralization efficiency of biogenic opal adjusted such that the overall steady state amount of silicon residing within the ocean was 9.5 × 10^{16} moles, which is equivalent to an average silicon concentration of 70 μmol L^{-1} [*Treguer et al.*, 1995]. For germanium, we set the input flux to 9.5 × 10^{6} moles yr^{-1}, composed of four sources: riverine (3.0 × 10^{6} moles yr^{-1}), hydrothermal (6.0 × 10^{6} moles yr^{-1}), submarine weathering (0.2 × 10^{6} moles yr^{-1}) and eolian (0.3 × 10^{6} moles yr^{-1}) [*Hammond et al.*, 2004]. Within the model we assumed that the loss of germanium from the ocean was via biogenic particles and via nonbiotic processes [*Hammond et al.*, 2000, 2004; *King et al.*, 2000]. For simplicity the nonbiotic process was treated as a first-order removal process and then adjusted such that at steady state the overall oceanic Ge:Si ratio equaled 0.76 × 10^{-6}; as observed in Figure 4. It should be noted that the nonbiotic germanium sink is actually a surface water removal process, but because it arises from silicon remineralization from sediments unaccompanied by germanium [*Hammond et al.*, 2000; *King et al.*, 2000], we chose to treat it as a first-order removal process independent of Si. The percentage of germanium lost via nonbiogenic processes is 45% assuming no fractionation.

[15] The next step was to incorporate Ge/Si fractionation into the model during opal formation. Ge/Si fractionation can be modeled based on three assumptions:

[16] 1. No Ge/Si fractionation occurs in surface waters.

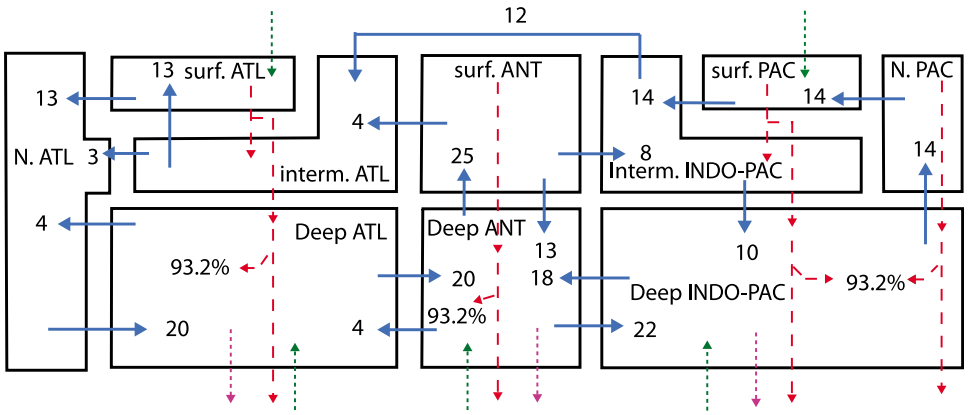

Figure 2. PANDORA 10 box model "which operates something like the real system" [*Broecker and Peng*, 1987]. Blue lines indicate water flow, and values are in Sv. Red lines indicate opal export from the surface ocean and are based on values from *Broecker and Peng* [1987]. Green lines indicate the four major oceanic germanium and silicon inputs (riverine, hydrothermal, eolian, and submarine weathering), whereas the purple arrow represents germanium loss via a nonbiological sink. The numbers in italics indicate the percentage of Si and Ge (with brackets) regenerated from biogenic opal dissolution within the water column and at the seafloor. Abbreviations for oceanic region are described as follows: North Atlantic (N.ATL), surface Atlantic (surf. ATL), intermediate Atlantic (Intermed. ATL), surface Antarctic (surf. ANT), intermediate Indo-Pacific (Intermed. INDO-PAC), surface Pacific (surf. PAC), North Pacific (N.PAC), deep Indo-Pacific (Deep INDO-PAC), deep Antarctic (Deep ANT), and deep Atlantic (Deep ATL).

[17] 2. Ge/Si fractionation occurs because there is a constant discrimination of germanium during opal formation [*Murnane and Stallard*, 1988; *Froelich et al.*, 1992]. This can be expressed as:

$$\mathrm{Ge/Si_{diatom}} = \mathrm{K_D} \cdot \mathrm{Ge/Si_{seawater}} \quad (1)$$

where $\mathrm{Ge/Si_{diatom}}$ is the Ge/Si of diatom frustules, $\mathrm{K_D}$ is the distribution coefficient, set to 0.5 [*Murnane and Stallard*, 1988] in the model, and $\mathrm{Ge/Si_{seawater}}$ is the Ge/Si of seawater with each surface box.

[18] 3. Ge/Si fractionation occurs during uptake by diatoms via a Michaelis-Menten process. This logic assumes that germanium uptake is passive to the silicon transport system but is taken up at a slower rate than silicon [*Ellwood et al.*, 2006]. The equation to describe this relationship is expressed as:

$$Ge/Si_{diatom} = \frac{V_{Ge}}{V_{Si}}.Ge/Si_{seawater} = \frac{\frac{V_{Ge_{max}}[Si]}{Km_{Ge}+[Si]}}{\frac{V_{Si_{max}}[Si]}{Km_{Si}+[Si]}}.Ge/Si_{seawater} \quad (2)$$

where $\mathrm{Km_{Ge}}$ and $\mathrm{Km_{Si}}$ are half-saturation constants for the uptake of germanium and silicon, respectively, $\mathrm{V_{Gemax}}$ and $\mathrm{V_{Simax}}$ are the maximum uptake rates for germanium and silicon, respectively, and [Si] is the concentration of silicon. Because it is assumed that both germanium and silicon are taken up via a single transport system and that germanium behaves like an isotope of silicon ($\mathrm{V_{Gemax}} = \mathrm{V_{Simax}}$.); in this expression the only difference between germanium and silicon are the half-saturation constants with $\mathrm{Km_{Ge}}$ being larger than $\mathrm{Km_{Si}}$ [*Ellwood et al.*, 2006].

3. Results

3.1. Germanium and Silicon Concentrations in Seawater

[19] Seventeen profiles of dissolved inorganic germanium concentration versus depth are presented in Figure 3 along with the corresponding depth profiles for dissolved silicon concentrations (see Data Set S1 for raw data).[1] The main feature of these profiles is an increase in germanium concentration, and hence silicon concentration, with depth. An additional feature of these profiles is the low concentrations of germanium and silicon in Atlantic samples compared to the South Pacific and Southern Ocean samples, which is consistent with previous germanium and silicon measurements for these oceanic basins. In addition, the Atlantic data showed that the more southern stations, e.g., PS69/26, had higher germanium concentrations at depth than the more northern stations. At station PS69/26, the influence of Antarctic Intermediate Water and Antarctic Bottom Water can be seen at about 1000 m and below 4000 m, respectively. The southward increase in germanium concentration is consistent with other nutrient measurements for this oceanic basin, e.g., nutrients' results from the GEOSECS program.

[1] Auxiliary materials are available at ftp://ftp.agu.org/apend/gb/2009GB003689.

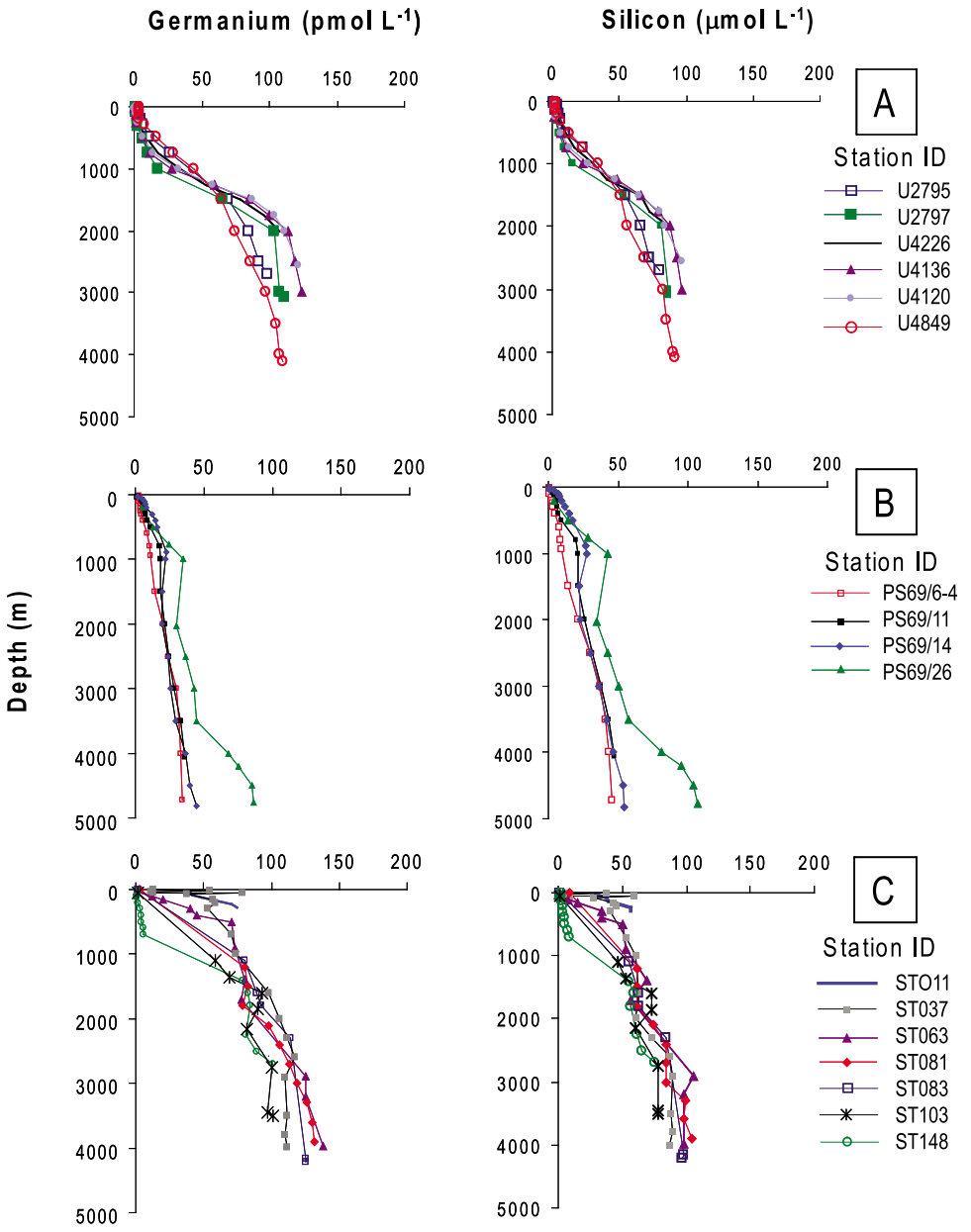

Figure 3. Depth profiles of dissolved inorganic germanium and silicon versus depth for (a) southwest Pacific Ocean, (b) Atlantic Ocean, and (c) Southern Ocean sites. Sample locations are indicated in legend adjacent to depth profiles.

[20] Using the seventeen profiles, the global oceanic relationship between dissolved germanium and silicon has been determined (Figure 4). Germanium and silicon concentrations are tightly coupled in oceanic water as can be seen by the strong positive relationship in Figure 4a (Ge = $0.760 \times 10^{-6} \pm 0.004$[Si] + 1.27 ± 0.24, $p < 0.001$, $r^2 = 0.993$). The regression on the Ge/Si data yields a positive germanium intercept that is not a function of analytical error or bias (uncertainty in blank is 0.6 ± 0.1 and scatter in data about the regression is greater than propagated error) and is consistent with published work [*Froelich et al.*, 1989; *Ellwood and Maher*, 2003]. The nonzero intercept for germanium requires that at relatively low silicon concentrations the Ge/Si will increase. Figures 4b and 4c highlight this relationship. For waters shallower than 1000 m (Figure 4b) and when silicon concentrations drop below ~10 μmol L^{-1} (Figure 4c) the Ge/Si increases indicating greater consumption of silicon by siliceous organisms relative to that of germanium.

[21] More detailed examination of the oceanic Ge/Si data suggests that the apparently strong linear relationship, mentioned above, curves at low concentrations (Figure 4d). In short, these data consistently show that waters low in silicon concentration (<10 μmol L^{-1}) sampled worldwide

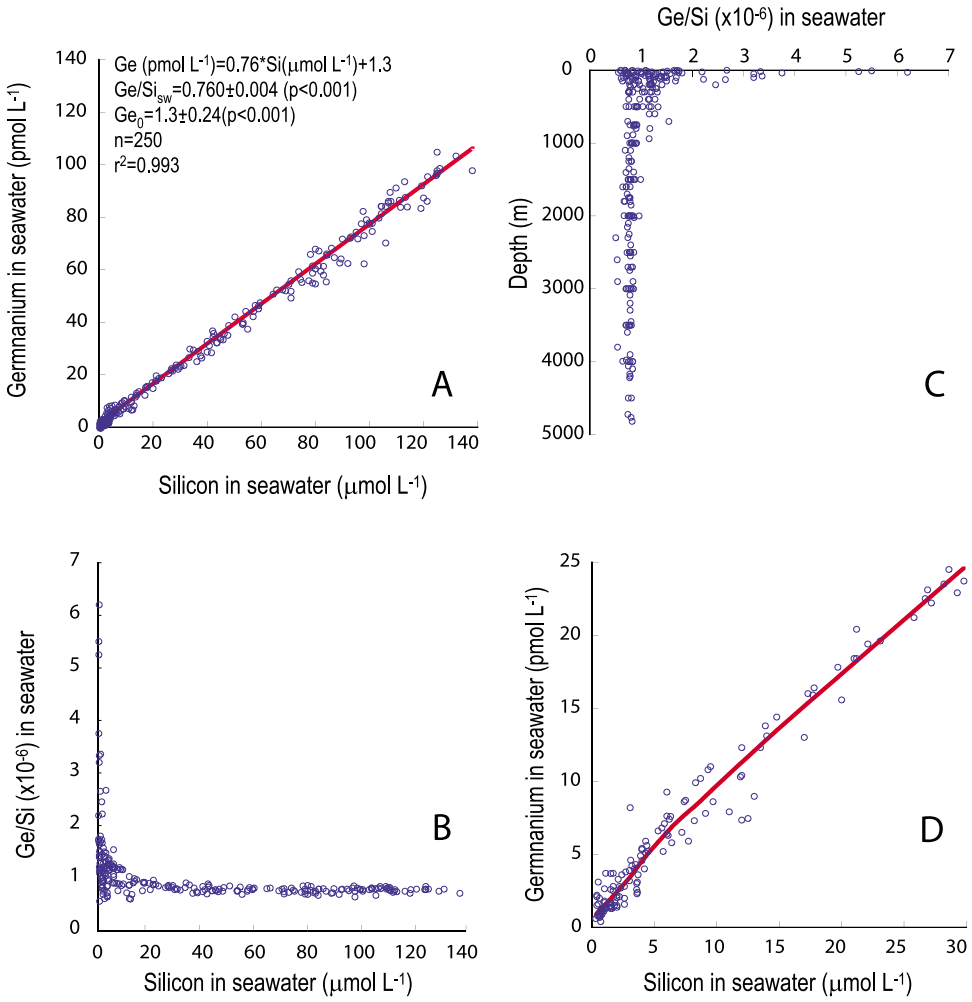

Figure 4. Global oceanic relationship of inorganic germanium versus silicon concentration. (a) Oceanic germanium versus silicon concentration (Ge = 0.760 × 10^{-6} ± 0.004[Si] + 1.27 ± 0.24, $p < 0.001$, r^2 = 0.993). (b) Ge/Si × 10^{-6} versus depth. (c) Ge/Si × 10^{-6} versus silicon concentration. (d) Oceanic germanium versus silicon concentration less than 25 pmol L^{-1} and 30 μmol L^{-1}, respectively. Curve is fitted using a second-order polynomial (r^2 = 0.99, $p < 0.001$).

have relatively more germanium than waters at higher silicon concentrations. The low silicon concentrations data fit to a weighted curve (second-order polynomial, r^2 = 0.99, $p < 0.001$) and appears to resolve the positive Ge intercept to near-zero at very low silicon concentrations.

[22] Enrichment of germanium is highlighted by comparing geographically distinct profiles that are either nutrient replete or deplete (Figure 5). Specifically Ge/Si depth profiles north (Figure 5a) and south (Figure 5b) of the Antarctic Polar Front (APF), respectively. Surface waters low in silicon are relatively enriched in germanium, e.g., station ST148 located in the subantarctic zone, whereas surface waters high in silicon are not germanium-enriched, e.g., stations located south of the APF (ST011, ST037, ST063, ST081, ST083, ST103). Profiles for the Atlantic and the southwest Pacific oceans (Figures 5c and 5d) reveal a similar pattern with germanium-enriched relative to that of silicon in surface waters.

3.2. Germanium and Silicon in Diatoms

[23] Coupled diatom and seawater Ge/Si data from the Southern Ocean are plotted versus silicon concentration are presented in Figure 6. The Ge/Si in seawater becomes higher as the concentration of silicon decreases (see Figure 4b for worldwide signal), whereas the diatom Ge/Si remains constant (Figure 6). Furthermore, the data clearly show a strong association between diatom and seawater Ge/Si when dissolved silicon concentrations are above 5 μmol L^{-1}. However, the diatom Ge/Si sharply deviates from the seawater Ge/Si below a dissolved silicon concentration of 5 μmol L^{-1}. At this low silicon concentration the diatoms maintain a Ge/Si of on average 0.78 (±0.02) × 10^{-6} while the surrounding waters have a Ge/Si of 1.17 (±0.10) × 10^{-6} to 7.46 (±0.80) × 10^{-6} (see Table 2). The only mechanism to adequately describe these data would require that diatoms discriminate against germanium when dissolved silicon concentrations are low.

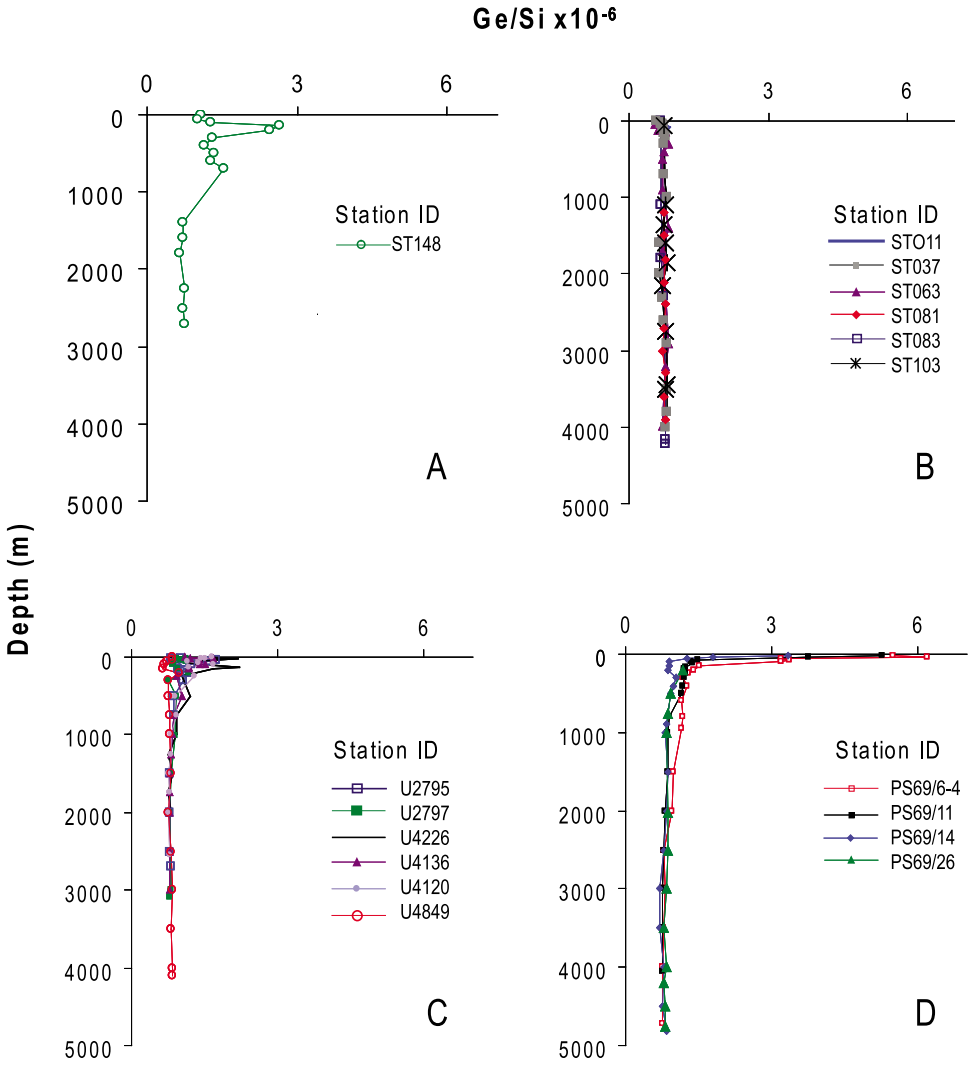

Figure 5. Ge/Si versus depth profiles for (a) Southern Ocean profiles low in Si (adjacent to Tasmania, $n = 2$), (b) Southern Ocean profiles high in Si (south of Antarctic Polar Front (APF), $n = 5$), (c) southwest Pacific Ocean profiles ($n = 6$), and (d) Atlantic Ocean profiles ($n = 4$).

[24] The average Ge/Si for diatoms did not vary from a value of 0.78×10^{-6} (std. error of all the samples is similar to the analytical error of ±0.02), and is within error of the global oceanic Ge/Si of 0.76×10^{-6}. An increase in germanium discrimination at low silicon is consistent with model results of the global data set. The diatom size fraction of 11–40 μm does reflect seawater Ge/Si at higher silicon concentrations (>5 μmol L^{-1}) but at lower silicon concentrations it does not. One possibility is that fragments from larger diatoms (>40 μm) and/or silicoflagellates, that are known to strongly discriminate against germanium [*Froelich et al.*, 1989], were dissolved, even though care was taken to avoid this situation.

[25] In order to investigate this apparent discrimination further, Figure 7 presents the observed K_D values (0.16–1.05) with four possible models to describe the data. Also presented are the locations of the Subantarctic Front (SAF) and the Antarctic Polar Front (APF) (with respect to measured silicon values). The observed data shows large K_D values for samples collected in a low-silicon environment (<5 μmol L^{-1}) as opposed to samples collected from a high-silicon environment (>5 μmol L^{-1}). The predicted values presented in Figure 7a assume that the Km for both germanium and silicon is the same and yields a model that would have no observable fractionation between seawater and diatoms. This model clearly does not fit the observed data. Figures 7b–7d present models that assume variable fractionation of Ge/Si based on changing the Km values for both germanium and silicon. The predicted values presented in Figure 7d appear to best fit that observed values, however, experimental evidence is required in order to establish whether these Km values are appropriate and can be used.

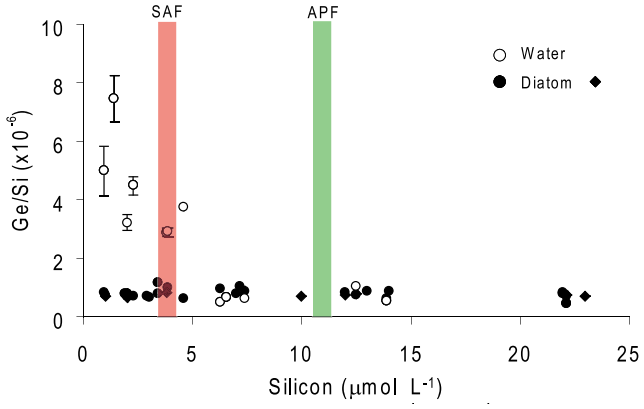

Figure 6. Diatom and seawater Ge/Si $\times 10^{-6}$ for samples collected along the SR3 transect between Tasmania, Australia, and Antarctica in the Southern Ocean. Two sets of diatom data are presented on the basis of summer (V3, black circles) and autumn (V6, black triangles) collection. The locations of the Subantarctic Front (SAF) in red and Antarctic Polar Front (APF) in green are identified (with respect to measured silicon values).

3.3. Modeling Ge/Si Fractionation Using PANDORA

[26] The following is based on the steady state results using three fractionation scenarios modeled using a 10 box model (Figure 8 and Table 3).

[27] When no fractionation is assumed (Figure 8a) the mode produces a linear relationship with small fractionation away from the global ratio 0.76×10^{-6}. For the surface Atlantic, intermediate Indo-Pacific and the intermediate Atlantic, Ge/Si ratios were below the global average, whereas for the North Atlantic and deep Atlantic boxes, Ge/Si ratios were above the global average (Table 3). A plot of germanium versus silicon produced a linear relationship with small positive intercept ($Ge = 0.758 \times 10^{-6} \pm 0.003[Si] + 0.08 \pm 0.16$, $r^2 = 1.00$). While an intercept and variations in water Ge/Si are produced these are due to the differences in the Ge/Si for respective source inputs and the large non-biotic germanium sink. *Hammond et al.* [2004] indicated that a significant portion of germanium is lost along coastal margins; however, the 10 box model used here does not simulate marginal processes very well, hence, we simulated these losses as occurring in deep waters, i.e., the deep Atlantic, Antarctic and Pacific. As a sensitivity analysis we

Table 2. Diatom and Water Concentration Data for Germanium ([Ge]), Silicon ([Si]), and Ge/Si[a]

		Diatom				Water			
Voyage/ID	Latitude	[Ge] (pmol L^{-1})	[Si] (μmol L^{-1})	Ge/Si	Error	[Ge] (pmol L^{-1})	[Si] (μmol L^{-1})	Ge/Si	Error
V3/152	−67	18,900	22,600	0.834	0.017		22.0		
V3/148	−66.6	21,400	26,500	0.810	0.016		22.0		
V3/69	−66.4	71,300	83,500	0.854	0.017		22.0		
V3/460	−66	8,890	12,200	0.440	0.015	10	22.1	0.471	0.013
V3/485	−66	16,400	21,300	0.773	0.015		22.0		
V6/18	−65.1	25,200	33,400	0.756	0.015		22.1		
V6/23	−64.2	20,200	28,300	0.712	0.014		23.0		
V3/590	−63.9	3,490	4,040	0.864	0.017		14.0		
V3/345	−63.2	4,010	6,600	0.608	0.012	8	13.9	0.558	0.022
V3/underway	−63.1	1,230	1,400	0.880	0.018		13.0		
V3/underway	−61	9,280	12,500	0.740	0.015	13	12.5	1.03	0.026
V6/58	−60	17,400	22,100	0.788	0.016		12.5		
V6/58	−59	25,700	33,400	0.770	0.015		12.0		
V3/underway	−58	8,980	10,800	0.834	0.017	31	12.0	2.55	0.06
V3/underway	−57	8,490	9,790	0.465	0.017	5	7.4	0.624	0.041
V6/underway	−56.9	23,500	33,300	0.706	0.014		10.0		
V6/81	−56	6,870	8,390	0.819	0.016	11	3.8	2.88	0.13
V3/underway	−55	4,120	4,310	0.450	0.019	3	6.3	0.515	0.048
V3/underway	−54.1	5,170	7,690	0.673	0.013	5	6.6	0.680	0.046
V3/underway	−54	9,880	12,600	0.784	0.016		7.0		
V3/underway	−53.4	3,410	4,580	0.746	0.015	6	2.0	3.22	0.27
V3/underway	−52.8	6,040	4,740	0.808	0.016	4	3.4	1.17	0.10
V3/underway	−52.1	13,300	13,300	1.001	0.02	11	3.8	2.90	0.13
V3/underway	−51	8,230	7,970	1.032	0.021	80*	7.2	11.2	0.2
V3/underway	−51	888	1,380	0.643	0.013	17	4.6	3.75	0.13
V3/underway	−50.6	2,550	3,910	0.652	0.013		3.0		
V3/underway	−50	431	607	0.711	0.014	41*	2.9	14.0	0.7
V3/underway	−48.6	1,230	1,550	0.798	0.016	14	1.9	7.46	0.80
V6/142	49	7,330	9,430	0.777	0.016	50*	2.3	21.7	1.7
V3/underway	−47.7	688	974	0.706	0.014	10	2.3	4.49	0.31
V3/underway	−47.1	298	381	0.782	0.016		2.0		
V6/underway	−46.2	1,940	2,810	0.691	0.014		1.0		
V3/underway	−45.1	545	710	0.769	0.015		1.0		
V3/underway	−44.9	12,900	15,800	0.818	0.016	5	0.9	5.01	0.84

[a]Voyage/ID identifies the research voyage and station ID for collected samples. Samples were collected over a summer voyage (V3) and an autumn voyage (V6). Several samples were not collected at a particular station and have been described as underway. Errors presented here represent the reproducibility error for Ge/Si. See section 2 for reproducibility of germanium and silicon analyses in oceanic waters and diatoms. Asterisk denotes potentially contaminated sample (not included in discussion).

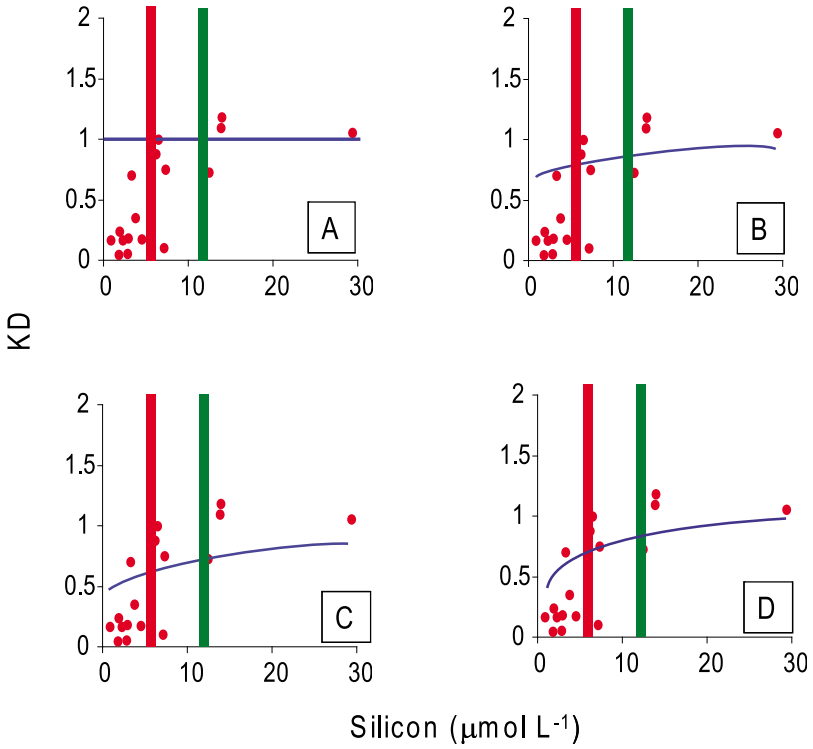

Figure 7. Four models presenting observed (red dots) and predicted (blue line) values for fractionation (K_D) based on a Micahelis Menten process. Predicted values presented were determined by varying the half-saturation constant (Km) for both germanium (Km_{Ge}) and silicon (Km_{Si}). The locations of the SAF in red and APF in green are identified (with respect to measured silicon values). (a) No fractionation ($K_D = 1$) $Km_{Si} = 5$ μmol L^{-1}, $Km_{Ge} = 5$ μmol L^{-1}. (b) Variable fractionation, $Km_{Si} = 5$ μmol L^{-1}, $Km_{Ge} = 9$ μmol L^{-1}. (c) Variable fractionation, $Km_{Si} = 5$ μmol L^{-1}, $Km_{Ge} = 12$ μmol L^{-1}. (d) Variable fractionation, $Km_{Si} = 0.5$ μmol L^{-1}, $Km_{Ge} = 4$ μmol L^{-1}.

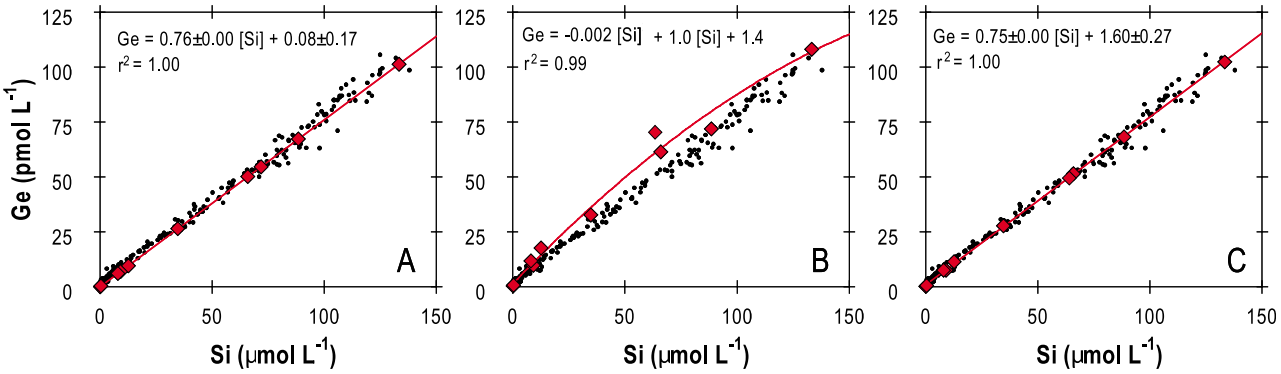

Figure 8. Model output based on the PANDORA 10 box model assuming (a) no fractionation, (b) fractionation using a constant fractionation factor ($K_D = 0.5$) (equation (1)), and (c) fraction occurring as result of a Michaelis-Menten process (equation (2)) using inputs of $Km_{Si} = 0.5$ μmol L^{-1} and $Km_{Ge} = 4$ μmol L^{-1}. If these values are changed to $Km_{Si} = 5$ μmol L^{-1} and $Km_{Ge} = 9$ μmol L^{-1} or $Km_{Si} = 5$ μmol L^{-1} and $Km_{Ge} = 12$ μmol L^{-1}, the following linear relationships ($r^2 = 1.00$, $p < 0.001$) are obtained, respectively: Ge = 0.76 ± 0.00[Si] + 0.99 ± 0.32 and Ge = 0.76 ± 0.00[Si] + 1.64 ± 0.49. Black dots represent observed germanium and silicon values, whereas the red line and red diamonds reflect the model output.

Table 3. Model Output Results From the 10 Box Model[a]

			Ge:Si ($\times 10^{-6}$)						
				No Fractionation		Rayleigh Fractionation	Michaelis-Menten Fractionation[b]		
Oceanic Region	Box	Si (μmol L^{-1})	Observed	Ge Loss Via Deep Ocean Boxes[c]	Ge Loss Intermediate Boxes[d]	K_D = 0.5	Km_{Si} = 5 μmol L^{-1}; Km_{Ge} = 9 μmol L^{-1}	Km_{Si} = 5 μmol L^{-1}; Km_{Ge} = 12 μmol L^{-1}	Km_{Si} = 0.5 μmol L^{-1} Km_{Ge} = 4 μmol L^{-1}
North Atlantic	1	11	nd	0.77	0.70	1.06	0.82	0.86	0.88
Surface Atlantic	2	0.2	1–3	0.68	0.58	2.75	1.33	1.89	4.41
Intermediate Atlantic	3	13	~1	0.75	0.61	1.39	0.88	0.97	0.91
Surface Antarctic	4	66	0.7	0.76	0.77	0.93	0.78	0.79	0.78
Intermediate Indo-Pacific	5	9	0.78	0.73	0.58	1.47	0.89	0.99	0.94
Surface Pacific	6	0.3	~2	0.76	0.77	2.15	1.36	1.83	3.91
North Pacific	7	64	0.7–0.8	0.76	0.77	1.08	0.78	0.80	0.78
Deep Indo-Pacific	8	130	0.71	0.76	0.77	0.81	0.76	0.76	0.76
Deep Antarctic	9	89	0.73	0.76	0.77	0.81	0.77	0.77	0.77
Deep Atlantic	10	40	0.75	0.78	0.74	0.94	0.80	0.82	0.82

[a]Model is based on PANDORA. Observed data and the three model outputs: (1) without fractionation (K_D = 1), (2) with fractionation using a constant fractionation factor (K_D = 0.5), and (3) with fractionation occurring as result of a Michaelis-Menten processes are presented here; nd, no data.
[b]Km_{Si} and Km_{Ge} values taken from Figure 7.
[c]Nonopal germanium losses occur in the deep Indo-Pacific, deep Antarctic, and deep Atlantic boxes.
[d]Nonopal germanium losses occur in the intermediate Indo-Pacific and intermediate Atlantic boxes.

also simulated germanium loss from the intermediate Indo-Pacific and the intermediate Atlantic boxes. This produced lower Ge/Si in all the Atlantic boxes and the intermediate Indo-Pacific box (Table 3). However, a plot of germanium versus silicon produced a linear relationship but with a negative intercept ($Ge = 0.776 \times 10^{-6} \pm 0.006[Si] - 0.95 \pm 0.36$, $r^2 = 1.00$). These results show that PANDORA is sensitive to the location of germanium inputs and losses within the model. However, in all runs the Ge/Si of each box were either close to the global 0.76×10^{-6} ratio or lower; with none of the model ratios nearing values measured for in surface waters (Figures 5 and 6).

[28] When fractionation is introduced using a constant fractionation factor (K_D = 0.5), a curved germanium versus silicon concentration relationship was obtained (Figure 8b), consistent with that reported by *Froelich et al.* [1992], but clearly it does not fit the observed data. A nonzero intercept for the germanium versus silicon concentration relationship is produced. Using this model, only 4 of the 10 respective oceanic regions can be adequately described (Table 3).

[29] When the model was run with Ge/Si fractionation occurring as result of Michaelis-Menten processes, a linear relationship is obtained along with a positive nonzero germanium intercept (Figure 8c). The nonzero intercept is significant and is similar in magnitude to the size of the intercept obtained from the observed data set. In addition, the Ge/Si produced are similar for measured ratios within the global ocean data set (Table 3).

4. Discussion

4.1. Ge/Si in the Ocean

[30] When germanium concentrations are plotted versus silicon concentrations a near-linear relationship is usually obtained for open ocean water samples (Figure 8). However, in all of these open ocean data sets published to date, a positive intercept almost always occurs, although the size of the intercept is variable with values ranging between 1.15 and 8.07 pmol L^{-1} [*Ellwood and Maher*, 2003; *Froelich and Andreae*, 1981; *Froelich et al.*, 1989; *McManus et al.*, 2003; *Mortlock and Froelich*, 1996; *Santosa et al.*, 1997]. While some of these intercept values come from older data sets obtained using the less sensitive hydride generation atomic adsorption spectrometry technique, which may have contained a hidden internal blank [*Mortlock and Froelich*, 1996], intercept values obtained for data sets generated using the more sensitive HG-ICP-MS technique also produced a statistically nonzero values. Such a nonzero intercept, whatever the measurement technique used, has been inferred as evidence for germanium discrimination during silicon uptake by siliceous organisms [*Murnane and Stallard*, 1988].

4.2. Ge/Si Discrimination by Diatoms

[31] At silicon concentrations below ~5 μmol L^{-1} the Ge/Si increases significantly indicating potential significant germanium discrimination by phytoplankton as silicon is consumed. In the young, nutrient-depleted North Atlantic waters (Figure 5), the Ge/Si for the upper water column is well above the value of 0.76 obtained from the global germanium versus silicon relationship (Figure 4a). This enrich-

ment is consistent with the prediction of *Ellwood and Maher* [2003] who suggested that Ge/Si fractionation in the ocean should be most obvious in the young nutrient-depleted waters of the Atlantic Ocean. A plot of Ge/Si versus silicon concentration (Figure 4b) also highlights that there is significant Ge/Si fractionation as the concentration of silicon decreases.

[32] The Ge/Si results for diatoms collected along a silicon gradient (Figure 6) also show that small diatoms (11–40 μm) do not reflect the seawater Ge/Si at very low concentrations of silicon (<5 μmol L^{-1}). These data show that diatoms will preferentially strip silicon from the water, relative to germanium, in order to build their frustules. It is known that large diatoms as well as other siliceous organisms (silicoflagellates and sponges) discriminate against germanium [*Froelich et al.*, 1989; *Ellwood et al.*, 2006]. The most likely mechanism leading to Ge/Si fractionation is discrimination against germanium during silicon uptake, especially when silicon concentrations are growth limiting.

[33] An argument in support of the physiological control of silicon and germanium uptake is not new. *Thamatrakoln and Hildebrand* [2008] presented empirical evidence suggesting that diatoms used two different systems for the uptake of both silicon and germanium. The first system suggested that both germanium and silicon uptake relied completely on active transport by silicon transporters when external silicon concentrations were low (<10 μmol L^{-1}). However, the concentration of silicon relative to germanium was much higher within the diatom than the media in which they grew. This evidence simply reaffirmed the view that germanium is a competitive inhibitor of silicon metabolism at the site of silicon transport [*Azam et al.*, 1973; *Azam and Volcani*, 1974; *Simpson et al.*, 1979; *Puerner et al.*, 1990]. The second system presented by *Thamatrakoln and Hilderbrand* [2008] employs diffusion as a mechanism to control silicon uptake, based on the concentration gradient between the extracellular and intracellular pools, when external silicon concentrations were high (>30 μmol L^{-1}). They discovered that in the second system that both germanium and silicon were nonsaturable with the relative concentrations within the cell accurately reflecting the concentrations outside of the cell. Further evidence is required before proper assessment of the mechanism behind discrimination is understood but most of the evidence presented herein points to Ge/Si fractionation occurring during active silicon transport into the cell.

4.3. Modeling Ge/Si Fractionation in the Ocean

[34] The modeling of Ge/Si fractionation during the biomineralization of opal has been typically described using a Rayleigh distillation model [*Froelich et al.*, 1992, 1989]. While this model has been used extensively to describe isotope fractionation, it is not necessarily appropriate to model germanium and silicon uptake by diatoms. Out of the three different assumptions for Ge/Si fractionation tested using the 10 box model (based on PANDORA) discussed herein, neither the Rayleigh distillation process (K_D = 0.5; see Figure 8b) nor the no fractionation (K_D = 1, see Figure 8a) assumption yielded a model that fit with the observed oceanic data set. The major drawback to using either the Rayleigh distillation or no fractionation assumptions is that the K_D between the solid and the aqueous phases remain constant.

[35] Out of the three assumptions presented, the only assumption to adequately describe the observed data assumed a Michaelis-Menten process with changes in K_D dependent on silicon concentration (Figure 8c). The assumption that Ge/Si fractionation is variable and dependent on silicon concentration was verified in Ge/Si discrimination by diatoms and has also been previously examined by *Ellwood et al.* [2006] in siliceous sponges. This result of silicon-dependent fractionation implies that diatoms physiologically control the assimilation, and therefore cycling, of germanium relative to silicon.

4.4. Implications of Ge/Si Fractionation for Paleoreconstruction of Silicon

[36] The Ge/Si record for core RC13–259 spanning the last 450,000 years shows systematic interglacial-glacial variations with interglacial frutusles having Ge/Si values of 0.7–0.8 × 10^{-6} and glacial frustules having Ge/Si values of 0.45–0.6 × 10^{-6} [*Mortlock et al.*, 1991; *Froelich et al.*, 1992]. Current thinking suggests that these interglacial-glacial Ge/Si fluctuations represent changes in the amount of germanium lost from the ocean via nonopaline sink [*Hammond et al.*, 2004, 2000; *King et al.*, 2000; *McManus et al.*, 2003]. However, these theories require the Ge/Si of fossil diatoms obtained from this Southern Ocean site to faithfully record changes in the seawater Ge/Si. Based on data presented in Figures 6 and 7, we believe that the Ge/Si record from the RC13–259 core site does indeed faithfully record the global seawater Ge/Si because it is unlikely the surface water silicon concentration at this site has dropped below about 10 μmol L^{-1}; the current surface water silicon concentration at this site is ~20 μmol L^{-1}. Thus Ge/Si fluctuations for this core site either represent changes in global inventory of silicon (increased during glacial times) or germanium (decreased during glacial times) or a combination of the both [*Froelich et al.*, 1992; *Hammond et al.*, 2004, 2000; *King et al.*, 2000; *McManus et al.*, 2003].

5. Conclusions

[37] Seventeen new germanium concentration profiles collected from the Atlantic Ocean, the southwest Pacific Ocean, and Southern Ocean show similar characteristics to those of silicon. When germanium concentration is plotted versus silicon concentration a near linear relationship was obtained with slope of 0.76 × 10^{-6} and an intercept of 1.27 pmol L^{-1}. However, when the Ge/Si × 10^{-6} was plotted versus depth or silicon concentration, higher values were observed in surface waters where silicon concentrations were low. Coupling seawater and diatom Ge/Si × 10^{-6} data provides evidence that germanium discrimination is occurring during silicon uptake by diatoms. Modeling of the germanium-silicon data set using a 10 box model presented suggests that the only type of fractionation to adequately describe the observed data result from a subtle difference during uptake via a Michaelis-Menten process. This implies

biological control over the uptake and therefore cycling of germanium and silicon in the ocean. This conclusion has obvious implications for paleonutrient reconstructions using the Ge/Si × 10^{-6}, the silicon isotope and the germanium isotope signatures of diatom opal.

[38] **Acknowledgments.** Financial support for the study was provided through a Royal Society of New Zealand Marsden Fund grant awarded to M.E. during his time at NIWA, New Zealand, the New Zealand Foundation for Research Science and Technology, the University of Canberra (Ecochemistry Laboratory), the Australian Research Council Discovery Project (DP0770820, DP0771519, awarded to M.E.), and the Deutsche Forschungsgemeinschaft (CR145/7-1 awarded to P.L.C.). A NSERC scholarship was awarded to J.S. We are grateful to the officers and crew of the RVs *Tangaroa*, *Aurora Australis*, and *Polarstern* for aid during seawater sample collection. We thank Stu Pickmere for silicon analysis of water samples collected on *Tangaroa* voyages. The *Polarstern* cruise was a preliminary German GEOTRACES cruise and special thanks goes to Michiel Rutgers van der Loeff (Chief Scientist, AWI), Uschi Hennings (IOW), and Gereon Budeus (AWI; for CTD data) for their help in our participation. Finally, we thank two anonymous reviewers for their thoughtful comments.

References

Azam, F., and B. E. Volcani (1974), Role of silicon in diatom metabolism, *Arch. Microbiol.*, *97*, 103–114, doi:10.1007/BF00403050.

Azam, F., B. B. Hemmingsen, and B. E. Volcani (1973), Germanium incorporation into the silica of diatom cell walls, *Arch. Microbiol.*, *92*, 11–20, doi:10.1007/BF00409507.

Bareille, G., M. Labracherie, R. A. Mortlock, E. Maier-Reimer, and P. N. Froelich (1998), A test of (Ge/Si)(opal) as a paleorecorder of (Ge/Si)(seawater), *Geology*, *26*(2), 179–182, doi:10.1130/0091-7613(1998)026<0179:ATOGSO>2.3.CO;2.

Broecker, W., and T.-H. Peng (1987), The role of CaCO3 compensation in the Glacial to interglacial atmospheric CO2 change, *Global Biogeochem. Cycles*, *1*(1), 15–29, doi:10.1029/GB001i001p00015.

DeMaster, D. J. (2002), The accumulation and cycling of biogenic silica in the Southern Ocean: Revisiting the marine silica budget, *Deep Sea Res., Part II*, *49*(16), 3155–3167, doi:10.1016/S0967-0645(02)00076-0.

Ellwood, M. J., and W. A. Maher (2002), An automated hydride generation-cryogenic trapping-ICP-MS system for measuring inorganic and methylated Ge, Sb and As species in marine and fresh waters, *J. Anal. At. Spectrom.*, *17*(3), 197–203, doi:10.1039/b109754g.

Ellwood, M. J., and W. A. Maher (2003), Germanium cycling in the waters across a frontal zone: The Chatham Rise, New Zealand, *Mar. Chem.*, *80*(2–3), 145–159, doi:10.1016/S0304-4203(02)00115-9.

Ellwood, M. J., M. Kelly, W. A. Maher, and P. De Deckker (2006), Germanium incorporation into sponge spicules: Development of a proxy for reconstructing inorganic germanium and silicon concentrations in seawater, *Earth Planet. Sci. Lett.*, *243*(3–4), 749–759, doi:10.1016/j.epsl.2006.01.016.

Filippelli, G. M., J. W. Carnahan, L. A. Derry, and A. Kurtz (2000), Terrestrial paleorecords of Ge/Si cycling derived from lake diatoms, *Chem. Geol.*, *168*(1–2), 9–26, doi:10.1016/S0009-2541(00)00185-6.

Froelich, P. N., and M. O. Andreae (1981), The marine geochemistry of Germanium: Ekasilicon, *Science*, *213*, 205–207, doi:10.1126/science.213.4504.205.

Froelich, P. N., R. A. Mortlock, and A. Shemesh (1989), Inorganic germanium and silica in the Indian ocean: Biological fractionation during $(Ge/Si)_{opal}$ formation, *Global Biogeochem. Cycles*, *3*, 79–88, doi:10.1029/GB003i001p00079.

Froelich, P. N., V. Blanc, R. A. Mortlock, S. N. Chillrud, W. Dunstant, A. Udomkit, and T.-H. Peng (1992), River fluxes of dissolved silica to the ocean were higher during the glacials: Ge/Si in diatoms, rivers and oceans, *Paleoceanography*, *7*, 739–768, doi:10.1029/92PA02090.

Hammond, D. E., J. McManus, W. M. Berelson, C. Meredith, G. P. Klinkhammer, and K. H. Coale (2000), Diagenetic fractionation of Ge and Si in reducing sediments: The missing Ge sink and a possible mechanism to cause glacial/interglacial variations in oceanic Ge/Si, *Geochim. Cosmochim. Acta*, *64*(14), 2453–2465, doi:10.1016/S0016-7037(00)00362-8.

Hammond, D. E., J. McManus, and W. M. Berelson (2004), Oceanic germanium/silicon ratios: Evaluation of the potential overprint of temperature on weathering signals, *Paleoceanography*, *19*, PA2016, doi:10.1029/2003PA000940.

Jin, K., Y. Shibata, and M. Morita (1991), Determination of germanium species by hydride generation inductively coupled argon plasma mass-spectrometry, *Anal. Chem.*, *63*(10), 986–989.

King, S. L., P. N. Froelich, and R. A. Jahnke (2000), Early diagenesis of germanium in sediments of the Antarctic South Atlantic: In search of the missing Ge sink, *Geochim. Cosmochim. Acta*, *64*(8), 1375–1390, doi:10.1016/S0016-7037(99)00406-8.

Koroleff, I. (1976), Analysis of micronutrients, in *Methods of Seawater analysis*, edited by K. Grasshof, pp. 134–145, Verlag-chimie, Berlin.

Kurtz, A. C., L. A. Derry, and O. A. Chadwick (2002), Germanium-silicon fractionation in the weathering environment, *Geochim. Cosmochim. Acta*, *66*(9), 1525–1537, doi:10.1016/S0016-7037(01)00869-9.

Lewis, B. L., P. N. Froelich, and M. O. Andreae (1985), Methylgermanium in natural-waters, *Nature*, *313*(6000), 303–305, doi:10.1038/313303a0.

Lewis, B. L., M. O. Andreae, P. N. Froelich, and R. A. Mortlock (1986), The geochemistry of germanium in natural-waters, *Abstr. Pap. Am. Chem. Soc.*, *192*, 133-GEOC.

Lewis, B. L., M. O. Andreae, P. N. Froelich, and R. A. Mortlock (1988), A review of the biogeochemistry of germanium in natural waters, *Sci. Total Environ.*, *73*(1–2), 107–120, doi:10.1016/0048-9697(88)90191-X.

Lewis, B. L., M. O. Andreae, and P. N. Froelich (1989), Sources and sinks of methylgermanium in natural waters, *Mar. Chem.*, *27*(3–4), 179–200, doi:10.1016/0304-4203(89)90047-9.

McManus, J., D. E. Hammond, K. Cummins, G. P. Klinkhammer, and W. M. Berelson (2003), Diagenetic Ge-Si fractionation in continental margin environments: Further evidence for a nonopal Ge sink, *Geochim. Cosmochim. Acta*, *67*(23), 4545–4557, doi:10.1016/S0016-7037(03)00385-5.

Mehard, C. W., C. W. Sullivan, F. Azam, and B. E. Volcani (1974), Role of silicon in diatom metabolism: 4. Subcellular localization of silicon and germanium in *Nitzschia alba* and *Cylindrotheca fusiformis*, *Physiol. Plant.*, *30*(4), 265–272, doi:10.1111/j.1399-3054.1974.tb03654.x.

Mortlock, R. A., and P. N. Froelich (1987), Continental weathering of germanium: Ge/Si in the global river discharge, *Geochim. Cosmochim. Acta*, *51*(8), 2075–2082, doi:10.1016/0016-7037(87)90257-2.

Mortlock, R. A., and P. N. Froelich (1996), Determination of germanium by isotope dilution hydride generation inductively coupled plasma mass spectrometry, *Anal. Chim. Acta*, *332*(2–3), 277–284, doi:10.1016/0003-2670(96)00230-9.

Mortlock, R. A., C. D. Charles, P. N. Froelich, M. A. Zibello, J. Saltzman, J. D. Hays, and L. H. Burckle (1991), Evidence for lower productivity in the Antarctic Ocean during the last glaciation, *Nature*, *351*(6323), 220–223, doi:10.1038/351220a0.

Mortlock, R. A., P. N. Froelich, R. A. Feely, G. J. Massoth, D. A. Butterfield, and J. E. Lupton (1993), Silica and germanium in Pacific Ocean hydrothermal vents and plumes, *Earth Planet. Sci. Lett.*, *119*(3), 365–378, doi:10.1016/0012-821X(93)90144-X.

Murnane, R. J., and R. F. Stallard (1988), Germanium fractionation during biogenic opal formation, *Paleoceanography*, *3*, 461–469, doi:10.1029/PA003i004p00461.

Puerner, N. J., S. M. Siegel, and B. Z. Siegel (1990), The experimental phytotoxicology of germanium in relation to silicon, *Water Air Soil Pollut.*, *49*(1–2), 187–195, doi:10.1007/BF00279520.

Santosa, S. J., S. Wada, H. Mokudai, and S. Tanaka (1997), The contrasting behaviour of arsenic and germanium species in seawater, *Appl. Organomet. Chem.*, *11*, 403–414, doi:10.1002/(SICI)1099-0739(199705)11:5<403::AID-AOC596>3.0.CO;2-4.

Shemesh, A., R. A. Mortlock, R. J. Smith, and P. N. Froelich (1988), Determination of Ge/Si in marine siliceous microfossils: Separation, cleaning and dissolution of diatoms and radiolaria, *Mar. Chem.*, *25*(4), 305–323, doi:10.1016/0304-4203(88)90113-2.

Shemesh, A., R. A. Mortlock, and P. N. Froelich (1989), Late Cenozoic Ge/Si record of marine biogenic opal: Implications for variations of riverine fluxes to the ocean, *Paleoceanography*, *3*, 221–234, doi:10.1029/PA004i003p00221.

Simpson, T. L., L. M. Refolo, and M. E. Kaby (1979), Effects of germanium on the morphology of silica deposition in a freshwater sponge, *J. Morphol.*, *159*, 343–354, doi:10.1002/jmor.1051590305.

Thamatrakoln, K., and M. Hildebrand (2008), Silicon uptake in diatoms revisited: A model for saturable and nonsaturable uptake kinetics and the

role of silicon transporters, *Plant Physiol.*, *146*(3), 1397–1407, doi:10.1104/pp.107.107094.

Treguer, P., D. M. Nelson, A. J. Vanbennekom, D. J. Demaster, A. Leynaert, and B. Queguiner (1995), The silica balance in the World Ocean: A reestimate, *Science*, *268*(5209), 375–379, doi:10.1126/science.268.5209.375.

P. L. Croot, FB2: Marine Biogeochemistry, IFM-GEOMAR, Leibniz-Institut für Meereswissenschaften, Düsternbrooker Weg 20, D-24105, Kiel, Germany. (pcroot@ifm-geomar.de)

M. J. Ellwood and J. Sutton, Research School of Earth Sciences, Australian National University, Canberra, ACT 0200, Australia. (jill.n.sutton@gmail.com)

W. A. Maher, Ecochemistry Laboratory, Applied Science and Institute for Applied Ecology, University of Canberra, Canberra, ACT 2601, Australia. (bill.maher@canberra.edu.au)